Department of Mathematics and Systems Analysis

Solution of coupled acoustic eigenvalue problems

Antti Ojalammi

Aalto University

DOCTORAL DISSERTATIONS

Aalto University publication series
DOCTORAL DISSERTATIONS 151/2020

Solution of coupled acoustic eigenvalue problems

Antti Ojalammi

A doctoral dissertation completed for the degree of Doctor of Science (Technology) to be defended, with the permission of the Aalto University School of Science, at an examination held at the lecture hall M1, and also via remote technology, on 13th November 2020 at 12.

Aalto University
School of Science
Department of Mathematics and Systems Analysis
Speech & Math

Supervising professor
Assistant Professor Antti Hannukainen, Aalto University. Finland

Thesis advisor
Dr. Jarmo Malinen, Aalto University, Finland

Preliminary examiners
Maseeh Professor Jeffrey S. Ovall, Portland State University, USA
Associate Professor Lothar Nannen, TU Wien, Austria

Opponent
Assistant Professor Kathrin Smetana, University of Twente, Netherlands

Aalto University publication series
DOCTORAL DISSERTATIONS 151/2020

ISBN 978-952-64-0066-2 (printed)
ISBN 978-952-64-0067-9 (pdf)
ISSN 1799-4934 (printed)
ISSN 1799-4942 (pdf)
http://urn.fi/URN:ISBN:978-952-64-0067-9

Unigrafia Oy
Helsinki 2020

Finland

Printed matter
4041-0619

Aalto University

Abstract

Aalto University, P.O. Box 11000, FI-00076 Aalto www.aalto.fi

Author
Antti Ojalammi

Name of the doctoral dissertation
Solution of coupled acoustic eigenvalue problems

Publisher School of Science

Unit Department of Mathematics and Systems Analysis

Series Aalto University publication series DOCTORAL DISSERTATIONS 151/2020

Field of research Mathematics

Manuscript submitted 10 June 2020 **Date of the defence** 13 November 2020

Permission for public defence granted (date) 20 August 2020 **Language** English

☐ **Monograph** ☒ **Article dissertation** ☐ **Essay dissertation**

Abstract

This thesis concerns the solution of finite element discretised Laplacian eigenvalue problems of coupled systems. A relevant application is studying human speech, where vowels are classified according to the lowest resonant frequencies of the vocal tract during sustained pronunciation. When computing these frequencies, the acoustic environment has to be accounted for. In this thesis, the vocal tract is considered as an interior system that is coupled with its acoustic environment, the exterior system. The coupling occurs through a fixed interface.

Models for computing the resonant frequencies are validated against data consisting of simultaneous MRI images and sound recordings. As the validation requires a large number of vocal tract geometries, an automatic extraction algorithm that generates vocal tract surface triangulations from MRI data is introduced. An instrument for performing frequency sweeps on physical models printed using these geometries was also modelled as a part of this thesis.

The confined space inside the head coil of the MRI machine creates an acoustic environment where mixed modes appear. That is, standing waves that oscillate both inside the oral cavity and the head coil are formed. Hence, it is important that the acoustic environment consisting of the MRI coil is accurately modelled when validating computational models. To efficiently solve relevant resonances related to different vocal tract geometries coupled with the unchanging MRI head coil, a method for reducing the computational complexity related to the fixed exterior system is introduced.

The mathematical observations related to the aforementioned method were generalised from an algebraic setting to a continuous Laplace eigenvalue problem. As a result, a theory for obtaining information on an eigenfunction in a local subdomain from localised boundary data was developed. The computational realisation of this theory is a domain decomposition type eigenvalue solver where tasks related to each subdomain are mutually independent. This method can be used to approximately solve finite element discretised eigenvalue problems where the number of degrees of freedom is prohibitively large for a single workstation to compute. Such an eigenvalue solver can be used to efficiently solve large eigenvalue problems without the need for a supercomputer. Due to the independence of computations related to subdomains, tasks can be sent over a network connection, making the method suitable for cloud computing environments.

Keywords acoustics, Helmholtz, eigenvalue, FEM, MRI, speech, domain decomposition

ISBN (printed) 978-952-64-0066-2 **ISBN (pdf)** 978-952-64-0067-9

ISSN (printed) 1799-4934 **ISSN (pdf)** 1799-4942

Location of publisher Helsinki **Location of printing** Helsinki **Year** 2020

Pages 138 **urn** http://urn.fi/URN:ISBN:978-952-64-0067-9

Tekijä
Antti Ojalammi

Väitöskirjan nimi
Kytkettyjen akustisten ominaisarvotehtävien ratkaiseminen

Julkaisija Perustieteiden korkeakoulu

Yksikkö Matematiikan ja systeemianalyysin laitos

Sarja Aalto University publication series DOCTORAL DISSERTATIONS 151/2020

Tutkimusala Matematiikka

Käsikirjoituksen pvm 10.06.2020 **Väitöspäivä** 13.11.2020

Väittelyluvan myöntämispäivä 20.08.2020 **Kieli** Englanti

☐ **Monografia** ☒ **Artikkeliväitöskirja** ☐ **Esseeväitöskirja**

Tiivistelmä

Tämä väitöskirja käsittelee elementtimenetelmällä diskretoitujen Laplace -operaattorin ominaisarvotehtävien ratkaisemista toisiinsa kytketyissä akustisissa systeemeissä. Tehtävä esiintyy erityisesti puheentutkimuksessa, jossa vokaaliäänteitä voidaan luokitella ääntöväylän alimpien resonanssitaajuuksien avulla. Näitä taajuuksia laskettaessa on huomioitava akustinen ympäristö. Tässä väitöskirjassa ääntöväylää käsitellään sisäsysteeminä, joka kytketään vakiorajapinnan yli ulkosysteemiin, eli ulkotilaan.

Resonanssitaajuuksien laskentaan käytettävät laskennalliset mallit validoidaan MRI-datan keräämisen yhteydessä tallennettujen ääninäytteiden avulla. Tämä vaatii suuren määrän ääntöväylägeometrioita, joten työssä esitellään automatisoitu menetelmä pinta- ja laskentaverkkojen luomiseen MRI-datasta. Lisäksi työssä mallinnetaan laite jolla voidaan mitata 3D-tulostettujen ääntöväylägeometrioiden taajuusvasteita.

MRI-laitteen pääkelan ahtaudesta johtuen äänitystilanteessa esiintyy seisovia aaltoja, jotka oskilloivat sekä pääkelan että ääntöväylän sisällä. Tästä syystä ulkotilan vaikutus täytyy mallintaa tarkasti. Jotta muuttumattomana pysyvän pääkelan vaikutus siihen kytkettyihin erilaisiin ääntöväylägeometrioihin voidaan mallintaa tehokkaasti, väitöskirjassa esitellään menetelmä laskennallisen vaativuuden vähentämiseksi tämänkaltaisissa tilanteissa.

Edelläkuvatun menetelmän kehittämisessä tehdyt huomiot yleistettiin algebrallisesta asetelmasta jatkuvalle Laplace -operaattorin ominaisarvotehtävälle. Näin saatiin teoreettinen menetelmä, jolla ominaisfunktion käytös paikallisessa alialueessa saadaan ratkaistua paikallisen reunakäytöksen avulla. Menetelmän laskennallinen toteutus on aluehajotukseen perustuva ominaisarvotehtävien ratkaisumenetelmä, jossa alialueisiin liittyvät laskentatyöt ovat toisistaan riippumattomia. Menetelmää voidaan käyttää elementtimenetelmällä diskretoitujen ominaisarvotehtävien approksimatiiviseen ratkaisemiseen silloin kun vapausasteiden määrä on liian suuri yksittäiselle tietokoneelle. Tällöin ei välttämättä tarvita suurteholaskentaa. Lisäksi laskentatehtävät voidaan lähettää verkon yli eri tietokoneille laskettavaksi, jolloin menetelmä soveltuu myös pilvilaskentaympäristöihin.

Avainsanat akustiikka, Helmholtz, ominaisarvo, FEM, MRI, puheentutkimus, aluehajotusmenetelmät

ISBN (painettu) 978-952-64-0066-2 **ISBN (pdf)** 978-952-64-0067-9

ISSN (painettu) 1799-4934 **ISSN (pdf)** 1799-4942

Julkaisupaikka Helsinki **Painopaikka** Helsinki **Vuosi** 2020

Sivumäärä 138 **urn** http://urn.fi/URN:ISBN:978-952-64-0067-9

Preface

This work was started under the supervision of Rolf Stenberg, but was transferred early on to the supervision of Antti Hannukainen, who along with my advisor Jarmo Malinen formed the driving force behind the completion of this thesis.

I wish to express my gratitude to my colleagues, friends (including the people of #k-metsä), and family for their sustained support along the years.

The TKK research foundation, Vilho, Yrjö and Kalle Väisälä foundation, the Academy of Finland projects with decision numbers 288980, 324611, and 312124 are wholeheartedly acknowledged for funding this work.

Helsinki, September 22, 2020,

Antti Ojalammi

Contents

List of Publications

This thesis consists of an overview and of the following publications which are referred to in the text by their Roman numerals.

I A. Ojalammi and J. Malinen. Automated segmentation of upper airways from MRI: Vocal tract geometry extraction. In *Proceedings of the 10th International Joint Conference on Biomedical Engineering Systems and Technologies*, Vol. 2. p. 77–84, 2017.

II A. Hannukainen, J. Kuortti, J. Malinen, and A. Ojalammi. An acoustic glottal source for vocal tract physical models. *Measurement Science and Technology*, Vol. 28, No. 11, 2017.

III J. Kuortti, J. Malinen, and A. Ojalammi. Post-processing speech recordings during MRI. *Biomedical Signal Processing and Control*, Vol. 39, pp. 11–22, 2017.

IV A. Hannukainen, J. Malinen, and A. Ojalammi. Efficient solution of symmetric eigenvalue problems from families of coupled systems. *SIAM Journal on Numerical Analysis*, Vol. 57, No. 4, pp. 1789—1814, 2018.

V A. Hannukainen, J. Malinen, and A. Ojalammi. PU-CPI solution of Laplacian eigenvalue problems. Submitted to *a journal*, arXiv: 2006.10427, June 2020.

Author's Contribution

Publication I: "Automated segmentation of upper airways from MRI: Vocal tract geometry extraction"

Ojalammi wrote the algorithm and created all illustrations except Figure 1. Both authors contributed to writing the article.

Publication II: "An acoustic glottal source for vocal tract physical models"

Ojalammi created the 3D illustrations, geometries, meshes, and performed the resonance analysis of the instrument with and without a vocal tract as load. Kuortti and Malinen wrote all other parts of the article.

Publication III: "Post-processing speech recordings during MRI"

Ojalammi wrote the parts of Section 6 related to solving the variational problem, created the 3D meshes, and computed the resonance modes and frequencies for each geometry. Kuortti and Malinen wrote all other parts of the article.

Publication IV: "Efficient solution of symmetric eigenvalue problems from families of coupled systems"

Ojalammi performed the numerical experiments. All authors contributed to writing the article.

Publication V: "PU-CPI solution of Laplacian eigenvalue problems"

Ojalammi performed the numerical experiments. All authors contributed to writing the article.

1. Introduction

This thesis studies numerical methods for solution of resonance problems related to pronunciation of vowels. Vowels, as all human speech, are produced by the vocal folds and the vocal tract. As air flows past the vibrating vocal folds, a periodic glottal pulse is generated. The vocal tract changes its shape to amplify certain frequency components of this pulse to produce different phonation. In the case of vowels, this means that a standing wave is formed in the vocal tract (VT) cavity corresponding to a certain frequency. As more energy is fed into the cavity in form of the glottal pulse, the amplitude of the standing wave increases. The interest then lies in finding out which frequencies get amplified given a vocal tract configuration.

Studying standing waves occurring in sustained phonation of vowels leads to an acoustic resonance problem. Our interest lies specifically in determining the three lowest resonance frequencies within the oral cavity, as each vowel can be distinguished based on them [4, 6]. Determining the resonant frequencies involves solving an eigenvalue problem related to a linear second order PDE. This PDE is typically discretised using Finite Element Method (FEM). Such is the case in Publications II and III, where speech production related resonance computations are carried out.

An essential component of computing resonances of the oral cavity is a geometric representation of the vocal tract. In our case, this means a connected mesh of tetrahedrons approximating the VT air volume. For this purpose, the VT is imaged using Magnetic Resonance Imaging (MRI). Our research group has been collecting 3D MRI data of different vowel configurations for several years, resulting in excess of a thousand samples from various test subjects [1]. Since the amount of data is too large for manual labour, there is a need for automated processing.

A tetrahedral mesh approximating the VT air volume can't be directly extracted from MRI data as there is no boundary for the VT at the open mouth. Instead, a surface mesh consisting of connected triangles approximating the boundaries of the VT air volume is extracted, see Figure 1.1. This is a non–trivial task, as is explained in Section 2. An automated

algorithm for this purpose is introduced in Publication I. In addition to

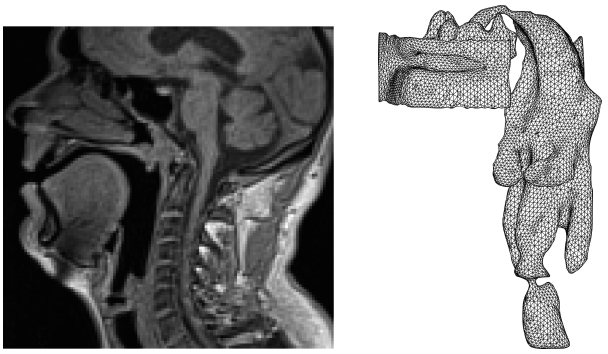

Figure 1.1. A sagittal plane from a 3D MR image, and the triangular surface mesh extracted from the full image.

computational speech modelling, surface meshes of vocal tracts can be used as models for additive manufacturing. This is demonstrated in Publication II, where frequency responses are measured from 3D printed vocal tract models.

A sufficiently fine FEM discretisation for observing the relevant phenomena in the model often results in equations with a large number of degrees of freedom, causing substantial computational costs and memory requirements. For instance, during MRI measurements, the test subject is lying inside an MRI machine, and the sound data is simultaneously recorded. An illustrative picture of the process is shown in Figure 2.1. In this case, the acoustic environment needs to be modelled in order to get a reasonable correspondence between characteristics of the recorded sound data and the computed resonances. However, the air volume inside the MRI head coil is significantly larger than the one in the vocal tract. As the environment also remains constant throughout the measurements, there is an incentive to pre-compute its effects on the resonances in order to reduce the complexity of computing the resonances of each vocal tract geometry.

In Publication IV, a domain decomposition method is introduced for pre-computing the effects of a subdomain interacting through an interface in numerical solution of eigenvalue problems. This is relevant when coupling multiple components into a system, see [11]. The method is based on approximating the eigenfunctions in a suitably chosen low-dimensional space.

In Publication V, the aforementioned method is refined into a parallel solver of FE-discretised eigenvalue problems. This method allows for distributed solution of eigenvalue problems using an arbitrary number of subdomains. Similar to the method in Publication IV, a low-dimensional basis is computed for each subdomain, and the bases are combined to form a global low-dimensional approximation space.

2. Medical imaging and vocal tract geometry extraction

Figure 2.1. Left: Preparing a subject for an MRI scan. The equipment for sound recording is being placed on the head coil. Right: An illustration of a vocal tract geometry coupled with an exterior acoustic geometry through a spherical interface shown in green.

We briefly discuss aspects related to obtaining a three-dimensional medical image of a VT. As subjects cannot be exposed to ionising radiation for non-clinical reasons, computed tomography, which is typically used when high resolution is needed, cannot be used. Ultrasound imaging is a harmless approach used, e.g., in tracking tongue movement [10]. Unfortunately, the low definition and the difficulties in imaging the entire VT makes this method infeasible.

MRI is a non-invasive imaging technique used in many clinical applications. As there is no ionising radiation involved, the procedure is safe to conduct on healthy patients in order to obtain control data, and to repeat the multiple times for the same subject, as is required when performing several instances of each vowel phonation.

The MRI data is stored as a three-dimensional array with a single intensity value for each element, or voxel, in the array. Additionally, the data contains information on the coordinates of each voxel, allowing for a correctly scaled reconstruction of the imaged object(s).

There are three challenges related to using MRI to obtain image data for

modelling vowel phonations. The first one is related to the physics of MRI: Only parts of the body containing water can be distinguished from air in the images, see [9]. As osseous tissue, such as bones and teeth, contains few water molecules, such tissue has poor contrast. For this reason, a significant challenge in extracting VT geometries from MR images is to prevent extracting the lower and upper jaw bone structures along with the VT air volume.

The second challenge with medical imaging is the fact that not every image is going to be perfect. More so in this case, where a strict protocol for the positioning of the patient does not exist, as an MRI of the vocal tract is not a standard procedure at the time of writing of this thesis. Additionally, phonation is by nature a non-static event, as the vocal folds are constantly vibrating. This along with the vibration of the uvula creates unavoidable motion artefacts.

The third challenge is related to coupling the extracted VT geometry to the exterior acoustic space, which is outlined in Sections 2.1 and 2.2.

2.1 Geometry extraction

As the goal of this thesis is to compute resonances of the vocal tract, it is necessary to first acquire three-dimensional computational geometries of the VT. For this purpose, Publication I describes an algorithm for extracting triangulated surfaces from Magnetic Resonance Imaging (MRI) data. The acquisition of this data is detailed in [1]. The same extraction algorithm is used in Publications II, III, and IV to produce the triangulated geometries used to generate tetrahedral meshes.

The previously used algorithm to extract a surface triangulation of the VT from the MRI data relied on manually extracted artefact models of the lower and upper jaws for each patient [2]. The artefact models were automatically aligned for every separate image, and the resulting air volume was extracted. The two challenges posed by this approach were the amount of manual labour required to construct the artefact models, as well as the challenges posed by the alignment process, since slight misalignment caused the extraction to fail substantially.

The approach discussed in Publication I was designed to be as robust as possible. Due to the large amount of MRI data available, it is preferable to extract a rough representation of the VT air volume from each sample so that the results can be studied in a statistical sense. The central idea in the algorithm is to refine a coarse binary voxel mask that blocks any osseous tissue while preserving the air volume of the VT. Pre-processing is applied to the MRI voxel data in order to increase contrast and improve edge definition. Coarse anatomical landmarks such as the location of the tip of the nose and the lower chin are used to estimate the location of

the mouth. An initial mask is created by iteratively smoothing the pre-processed image data and extracting a series of binary masks using seeded region growing. the surface area of the extracted masks are computed, and the change in surface area is monitored. A large change in the extracted surface area indicates that the tooth canals leading to the upper and lower jaw bones have been blocked.

The initial mask is then used up to a certain depth as a guide to obtain a more refined mask. This process is repeated using the most recently created mask and raising the threshold intensity as necessary until the mask contains the VT air volume at least up to the vocal folds.

2.2 Coupling with the exterior model

Due to the constrained space inside the MRI machine, particularly within the head coil, the acoustics of the MRI machine needs to be accounted for in the modelling process. To this end, we received a 3D CAD model of the Siemens Avanto head coil from Siemens Healthineers. A tetrahedral mesh of the air volume within the coil was created with a generic head model positioned inside, shown in Figure 4.1. In order to conveniently couple meshes of different vocal tract configurations with the exterior mesh, a spherical interface surface is placed around the mouth to act as a boundary of the exterior acoustic space. The extracted VT geometries were then stitched to a copy of this interface in order to connect the two meshes. Since generating the tetrahedral mesh of the VT is not a straightforward operation, some interface triangles may get removed during the process. Thus, it is convenient to use Nitsche's method and discretise the two meshes separately, as the interface surface triangulations need not match. This approach is used in Publication III.

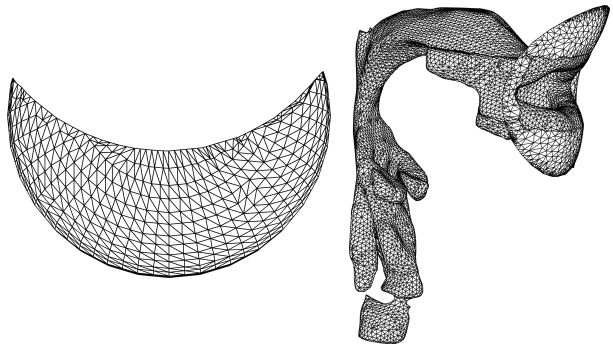

Figure 2.2. A top-down view of the interface and a triangulated VT geometry to which the interface is attached.

The VT surface model also needs to be processed in order to generate

a suitable mesh. A 2D triangulation is generated between the boundary edges of the interface and the boundary edges near the mouth of the extracted triangulated VT. An approximation of the facial features is obtained by solving a two-dimensional Poisson problem with a constant load and boundary conditions indicating the third coordinate. The spherical interface and an example of an extracted VT surface that is compatible with the interface are shown in Figure 2.2.

3. Acoustic eigenvalue problems

3.1 Helmholtz equation

We briefly present the two common PDE's in acoustics and their relation to each other. Let $\Omega \subset \mathbb{R}^d, d = 2, 3$ be a domain. The wave equation is a second order linear PDE,

$$c^2 \Delta p = \frac{\partial^2 p}{\partial t^2}, \quad \text{in } \Omega,$$

where c is the speed of sound in the media and $p = p(x, t)$ is a scalar field corresponding to the pressure deviation. This equation is used to model the propagation of waves in different media.

To study standing waves, we assume that the pressure field p is of the form $p(x, t) = \mathrm{e}^{i\omega t} u(x)$ where $\omega = 2\pi f$ is called the *angular frequency*. This is called the *time-harmonic ansatz*. Inserting the ansatz into the wave equation yields

$$c^2 \Delta u = -\omega^2 u, \quad \text{in } \Omega.$$

This is known as the *Helmholtz equation*. Denoting $\lambda = \omega / c$, we arrive at an eigenvalue problem: Find λ and u such that

$$\Delta u = -\lambda^2 u, \quad \text{in } \Omega. \tag{3.1}$$

Let $\partial\Omega = \Gamma_N \cup \Gamma_D \cup \Gamma_R$. The commonly used boundary conditions in speech modelling are homogeneous Neumann, homogeneous Dirichlet, and Robin boundary conditions, defined as

$$\begin{aligned} \frac{\partial u}{\partial n} &= 0, \quad \text{on } \Gamma_N, \\ u &= 0, \quad \text{on } \Gamma_D, \\ \frac{\partial u}{\partial n} + \lambda u &= 0, \quad \text{on } \Gamma_R, \end{aligned} \tag{3.2}$$

where $\Gamma_N,\ \Gamma_D$, and Γ_R denote the Neumann, Dirichlet, and Robin boundary sections, respectively.

3.2 Finite element discretisation

We now take a look at numerically solving the eigenvalue problem given in (3.1) with the boundary conditions (3.2). Since the acoustic eigenvalue problem is posed in a complicated domain, it is discretised using finite element method. FEM utilises the *variational formulation* of (3.1): Find $(\lambda, u) \in \mathbb{C} \times \mathcal{V}$ such that

$$\int_\Omega \nabla u \cdot \nabla v \,\mathrm{d}x + \lambda \int_{\Gamma_R} uv \,\mathrm{d}x = \lambda^2 \int_\Omega uv \,\mathrm{d}x, \quad \text{for all } v \in \mathcal{V} \subset H^1(\Omega). \tag{3.3}$$

The space $\mathcal{V}$ depends on the boundary conditions posed on the problem. For instance, a homogeneous Dirichlet condition $\partial\Omega = \Gamma_D$ results in $\mathcal{V} = H^1_0(\Omega)$, whereas Neumann boundary condition $\partial\Omega = \Gamma_N$ yields $\mathcal{V} = H^1(\Omega)$.

Robin type boundary conditions are relevant in acoustic applications. For instance, a boundary condition corresponding to Γ_R is posed at the termination of the trachea at or slightly below the vocal folds in VT resonance computations [3], as is done in Publication III. If $\Gamma_R \neq \emptyset$, (3.3) is a quadratic eigenvalue problem whose numerical solution and mathematical analysis is complicated. In this thesis, the case $\Gamma_R = \emptyset$ is considered for the sake of simplicity. Problem (3.3) then reduces to finding $(\mu, u) \in \mathbb{R}^+ \times \mathcal{V}$ such that

$$\int_\Omega \nabla u \cdot \nabla v \,\mathrm{d}x = \mu \int_\Omega uv \,\mathrm{d}x, \quad \text{for all } v \in \mathcal{V} \subset H^1(\Omega). \tag{3.4}$$

The eigenvalues are obtained from the relation $\mu = \lambda^2,\ \lambda \geq 0$.

Problem (3.4) is numerically solved using finite element method. In FEM, the space $\mathcal{V}$ is replaced by a finite dimensional space $\mathcal{V}_h \subset \mathcal{V}$. This yields the discretised problem: Find $(\lambda_h, u_h) \in \mathbb{R}^+ \times \mathcal{V}_h$ such that

$$\int_\Omega \nabla u_h \cdot \nabla v_h \,\mathrm{d}x = \lambda_h \int_\Omega u_h v_h \,\mathrm{d}x, \quad \text{for each } v_h \in \mathcal{V}_h. \tag{3.5}$$

As $\mathcal{V}_h$ we use the space of piecewise linear functions over a triangular ($d = 2$) or tetrahedral ($d = 3$) partition of Ω with basis $\{\varphi_j\}_{j=1}^n$, $\varphi_j : \Omega \to \mathbb{R}$. Expanding u_h and v_h in this basis, (3.5) is equivalent to

$$\mathsf{A}\mathbf{x} = \lambda_h \mathsf{M}\mathbf{x}, \tag{3.6}$$

where $\mathsf{A}, \mathsf{M} \in \mathbb{R}^{n\times n},\ \mathsf{A}_{ij} = \int_\Omega \nabla\varphi_j \cdot \nabla\varphi_i \,\mathrm{d}x,\ M_{ij} = \int_\Omega \varphi_j\varphi_i \,\mathrm{d}x$, are called the stiffness and mass matrices, respectively. If $\Gamma_D \neq \emptyset$, these matrices are sparse, symmetric, and positive definite. The vector $\mathbf{x} \in \mathbb{R}^n$ is the coordinate vector of the eigenfunction $u_h = \sum_{j=1}^n x_i\varphi_i$. The set of eigenvalues of (3.6) is denoted by $\sigma(\mathsf{A}, \mathsf{M})$.

Cholesky decomposition is used to transform (3.6) to a standard eigenvalue problem. For a symmetric positive definite matrix $\mathsf{A} \in \mathbb{R}^{n\times n}$, the (lower triangular) decomposition is

$$\mathsf{A} = \mathsf{L}\mathsf{L}^T.$$

Besides being efficient to compute, the decomposition also produces sparse matrices, although with some fill-in. This property is crucial when dealing with large sparse matrices due to memory constraints. Hence, Cholesky decomposition is commonly used to solve linear systems of equations. Problem (3.6) can be written as a standard eigenvalue problem using the Cholesky decomposition $\mathsf{M} = \mathsf{L}\mathsf{L}^T$:

$$\hat{\mathsf{A}}\mathbf{y} = \frac{1}{\lambda}\mathbf{y}, \quad \text{where} \quad \mathbf{y} = \mathsf{L}^T\mathbf{x}, \quad \hat{\mathsf{A}} = \mathsf{L}^T\mathsf{A}^{-1}\mathsf{L}. \tag{3.7}$$

Note that an inverse formulation is used in order to find the lowest eigenvalues of (3.6) when using power iteration.

3.3 Rayleigh-Ritz method

Modern eigenvalue solvers are typically of Ritz type. Given a generalised eigenvalue problem $\mathsf{A}\mathbf{x} = \lambda\mathsf{M}\mathbf{x},\ \mathsf{A},\mathsf{M} \in \mathbb{R}^{n\times n},\ \mathbf{x} \in \mathbb{R}^n$ where A and M are symmetric, positive definite matrices, the number of unkowns can be reduced at the cost of accuracy of the solution, or when the interest lies on eigenvalues within a specific interval. Let $\mathcal{W} \subset \mathbb{R}^n$, and $\{\mathbf{v}_j\}_{j=1}^k$ be a basis of $\mathcal{W}$. The Ritz eigenpairs $(\tilde{\lambda}, \tilde{\mathbf{x}}) \in \mathbb{R} \times \mathbb{R}^k$ are given by

$$\mathsf{V}^T\mathsf{A}\mathsf{V}\tilde{\mathbf{x}} = \tilde{\lambda}\mathsf{V}^T\mathsf{M}\mathsf{V}\tilde{\mathbf{x}}, \tag{3.8}$$

where we call $\mathsf{V} = \begin{bmatrix}\mathbf{v}_1, \dots, \mathbf{v}_k\end{bmatrix} \in \mathbb{R}^{n\times k}$ the *method matrix*, and $\mathcal{W}$ the *method subspace*. We denote the family of eigenvalues satisfying (3.8) by $\sigma_{\mathcal{W}}(\mathsf{A},\mathsf{M})$. Similarly, when $\{\mathbf{v}_j\}_{j=1}^k$ is an orthonormal basis, the standard eigenvalue problem (3.7) can be written in the subspace $\mathcal{W}$ as

$$\mathsf{V}^T\hat{\mathsf{A}}\mathsf{V}\tilde{\mathbf{y}} = \frac{1}{\tilde{\lambda}}\tilde{\mathbf{y}}. \tag{3.9}$$

The quality of the approximation of the pairs $(\tilde{\lambda}, \mathsf{V}\tilde{\mathbf{x}}) \in \mathbb{R}^+ \times \mathcal{W}$ compared to the eigenpairs of the original problem depends on the method subspace. An a priori error estimate for the relative eigenvalue error similar to [5] is used: Let $(\lambda, \mathbf{x})$ satisfy $\mathsf{A}\mathbf{x} = \lambda\mathsf{M}\mathbf{x}$ and $\mathbf{x}^T\mathsf{M}\mathbf{x} = 1$. There exists $\tilde{\lambda} \in \sigma_{\mathcal{W}}(\mathsf{A},\mathsf{M})$ such that

$$\frac{|\lambda - \tilde{\lambda}|}{\lambda} \leq C(\lambda) \min_{\mathbf{v}\in\mathcal{W}} \|\mathbf{x} - \mathbf{v}\|_{\mathsf{A}}^2, \tag{3.10}$$

where $\|\cdot\|_{\mathsf{A}} = \|\mathsf{A}^{1/2}\cdot\|_2$. The Rayleigh-Ritz method can also be used to approximately solve continuous eigenvalue problems, e.g., problem (3.3). One example is using FEM discretisation to approximate the eigenfunctions in a finite dimensional space. An essentially indentical error estimate to (3.10) is given in [5].

According to (3.10), the space $\mathcal{W}$ should be chosen to accurately approximate the eigenvectors corresponding to the eigenvalues of interest.

A useful example of the Rayleigh-Ritz method is given via Krylov spaces. For a matrix $\mathsf{A} \in \mathbb{R}^{n\times n},\ \mathbf{b} \in \mathbb{R}^n$, a Krylov space of degree k is defined as

$$\mathcal{K}_k(\mathsf{A}, \mathbf{b}) := span\{\mathbf{b}, \mathsf{A}\mathbf{b}, \mathsf{A}^2\mathbf{b}, \ldots, \mathsf{A}^{k-1}\mathbf{b}\}.$$

As k increases, the vector $\mathsf{A}^{k-1}\mathbf{b}$ approaches the eigenvector of A corresponding to its largest eigenvalue. The initial vector $\mathbf{b}$ is typically chosen randomly. When solving for the smallest eigenvalues, the space $\mathcal{K}_k(\mathsf{A}^{-1}, \mathbf{b})$ is used to compute their reciprocals. If A is a large and sparse matrix, computing its inverse is typically prohibitively expensive. Instead, a suitable factorisation of A is used to compute the vector $\mathsf{A}^{-1}\mathbf{v}$ using back substitution.

A Krylov subspace for computing the smallest eigenvalues is $\mathcal{K}_k(\hat{\mathsf{A}}^{-1}, \mathbf{b})$. Note that the Cholesky factor needs to be stored to recover the eigenvectors.

An orthogonal basis for the Krylov space is obtained using Arnoldi iteration. If A is Hermitian, the process leads to the Lanczos iteration, where the matrix $\mathsf{V}^*\mathsf{A}\mathsf{V} \in \mathbb{R}^{k\times k}$ is tridiagonal.

The a priori error bounds for the eigenvalues of the projected eigenvalue problem for the Lanczos iteration are discussed in [8]. In short, one needs to compute a larger dimensional Krylov space than the amount of largest eigenvalues sought for. For instance, Matlab uses a factor of 2 for the dimension.

4. Domain decomposition

The goal in Publications IV and V is to speed up the solution of (3.3) when the interest lies in eigenvalues on the *spectral interval of interest* $(0, \Lambda)$. An example of such a problem occurs when studying the pronunciation of

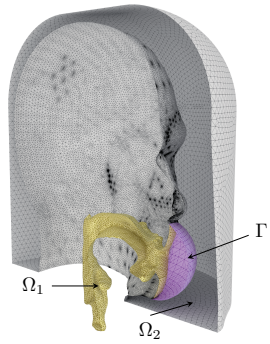

Figure 4.1. An example of a domain decomposition where a vocal tract is connected to an exterior acoustic space defined by the head and the MRI head coil. The joining interface is denoted by Γ.

vowels where the interest lies in the lowest resonant frequencies within the oral cavity. Both methods introduced in these publications are Ritz type domain decomposition methods. The domain Ω is split into smaller subdomains, and a local Ritz space is constructed separately for each subdomain. The method subspace is then obtained by combining the local Ritz spaces.

The local Ritz spaces are constructed using a representation mapping which expresses the eigenfunction u in a subdomain U as a λ-dependent linear mapping acting on $u|_{\partial\widehat{U}}$. Here $\widehat{U}$ is an extended subdomain related to U. Since the eigenvalues and eigenfunctions are unknown, the local Ritz space is obtained by studying the range of the representation mapping. Due to singularities with respect to λ, the representation mapping is split into singular and analytical parts. The range of the singular part is finite dimensional and easy to compute. The non-linearity of the analytical

part with respect to λ is treated with interpolation. We call this approach Condensed Pole Interpolation (CPI). The dimension of the local Ritz space is kept small using Singular Value Decomposition (SVD).

4.1 Condensed Pole Interpolation

We proceed to describe the CPI method using the setting of Publication IV. The domain Ω is decomposed into two subdomains such that

$$\Omega = \Omega_1 \cup \Omega_2.$$

In our speech acoustics application, the domain Ω_1 represents the vocal tract, while Ω_2 is the MRI head coil, see Figure 4.1. We are interested in solving the problem (3.3) using several different VT geometries and a fixed MRI head coil geometry. That is, Ω_1 is allowed to vary while Ω_2 remains unchanged. The computations are sped up by finding a low dimensional local Ritz space corresponding to Ω_2 while a trivial local Ritz space is used for Ω_1. In the CPI method, the extended subdomain related to Ω_2 is implicitly defined.

Problem (3.3) is discretised using FEM with tetrahedral elements and first order linear basis functions. Assuming that the degrees of freedom are ordered properly, Equation (3.6) can be written as

$$\begin{bmatrix} \mathsf{A}_{11} & \mathsf{A}_{12} \\ \mathsf{A}_{21} & \mathsf{A}_{22} \end{bmatrix} \begin{bmatrix} \mathbf{x}_1 \\ \mathbf{x}_2 \end{bmatrix} = \lambda \begin{bmatrix} \mathsf{M}_{11} & \mathsf{M}_{12} \\ \mathsf{M}_{21} & \mathsf{M}_{22} \end{bmatrix} \begin{bmatrix} \mathbf{x}_1 \\ \mathbf{x}_2 \end{bmatrix}, \quad \mathbf{x}_1 \in \mathbb{R}^{n_1},\ \mathbf{x}_2 \in \mathbb{R}^{n_2}, \tag{4.1}$$

where $\mathbf{x}_1$ and $\mathbf{x}_2$ are the coefficient vectors of the basis functions related to the subdomains Ω_1 and Ω_2, respectively. Since A_{22}, M_{22}, range(A_{21}), and range(M_{21}) are associated with the MRI head coil, they are assumed to not change as A_{11} and M_{11}, corresponding to the VT geometry, are allowed to vary. The CPI method matrix $\mathsf{Q} \in \mathbb{R}^{n\times(n_1+m)},\ m < n_2$, satisfies

$$\mathsf{Q} = \begin{bmatrix} \mathsf{I} & 0 \\ 0 & \mathsf{Q}_2 \end{bmatrix} \quad \text{where} \quad \mathsf{I} \in \mathbb{R}^{n_1\times n_1},\ \mathsf{Q} \in \mathbb{R}^{n_2\times m}. \tag{4.2}$$

The local Ritz space corresponding to Ω_2 is $\mathcal{V}_2 := range(\mathsf{Q}_2)$, and the method subspace is $\mathcal{V} :=$ range(Q). If $\mathcal{V}$ has the structure induced by (4.2), the estimate (3.10) gives

$$\frac{|\lambda - \tilde{\lambda}|}{\lambda} \leq C(\lambda) \min_{\mathbf{v}_2 \in \mathcal{V}_2} \|\mathbf{x}_2 - \mathbf{v}_2\|^2_{\mathsf{A}_{22}}, \quad \text{where} \quad \|\cdot\|_{\mathsf{A}_{22}} = \|\mathsf{A}_{22}^{1/2}\cdot\|_2. \tag{4.3}$$

According to (4.3), the local Ritz space $\mathcal{V}_2$ should approximate $\mathbf{x}_2$ for any $([\mathbf{x}_1^T\ \mathbf{x}_2^T]^T, \lambda) \in \mathbb{R}^n \times (0, \Lambda)$ satisfying (4.1) and of unit length in the norm induced by M. For this purpose, we study the representation formula derived from (4.1),

$$\mathbf{x}_2 = (\mathsf{A}_{22} - \lambda\mathsf{M}_{22})^{-1}(\lambda\mathsf{M}_{21} - \mathsf{A}_{21})\mathbf{x}_1, \quad \text{for} \quad \lambda \notin \sigma(\mathsf{A}_{22}, \mathsf{M}_{22}). \tag{4.4}$$

This formula can be exploited by noticing that the ranks of A_{21} and M_{21} are small. These matrix blocks are related to the coupling of the two subsystems.

We proceed to split the representation mapping $t \mapsto (\mathsf{A}_{22} - t\mathsf{M}_{22})^{-1}$ into analytical and singular parts. Let $(\mu_k, \mathbf{v}_k) \in \mathbb{R}^+ \times \mathbb{R}^{n_2}$ be an eigenpair of the pencil $(\mathsf{A}_{22}, \mathsf{M}_{22})$ satisfying

$$\mathbf{v}_i^T \mathsf{M}_{22} \mathbf{v}_j = \delta_{ij}, \quad \mathbf{v}_i^T \mathsf{A}_{22} \mathbf{v}_j = \mu_i \delta_{ij}. \tag{4.5}$$

The eigenvectors $\mathbf{v}_k$ form an M_{22}-orthonormal basis of $\mathbb{R}^{n_2}$. Define an M_{22}-orthogonal projection

$$\mathsf{P}_{\tilde{\Lambda}} := \sum_{k=1}^{K(\tilde{\Lambda})} \mathbf{v}_k \mathbf{v}_k^T \mathsf{M}_{22},$$

and split the representation mapping as

$$\mathbf{x}_2 = \sum_{k=1}^{K(\tilde{\Lambda})} \alpha_k \mathbf{v}_k + f_{\tilde{\Lambda}}(\lambda)(\lambda \mathsf{M}_{21} - \mathsf{A}_{21})\mathbf{x}_1, \tag{4.6}$$

where $f_{\tilde{\Lambda}}(t) := (\mathsf{I} - \mathsf{P}_{\tilde{\Lambda}})(\mathsf{A}_{22} - t\mathsf{M}_{22})^{-1}$ is the analytic part of the representation mapping. Define $E_{\tilde{\Lambda}} := \operatorname{span}(\{\mathbf{v}_1, \ldots, \mathbf{v}_{K(\tilde{\Lambda})}\})$, where $\tilde{\Lambda} > \Lambda$ and $K(\tilde{\Lambda}) := \#\{k \in \mathbb{N} \mid \mu_k < \tilde{\Lambda}\}$. Following (4.6), the method subspace is defined as $\mathcal{V}_2 = E_{\tilde{\Lambda}} \oplus \mathcal{W}_2$ where $\mathcal{W}_2$ is the *complementing subspace* approximating the space

$$\left\{ f_{\tilde{\Lambda}}(t)\mathbf{w} \;\middle|\; t \in (0, \Lambda),\ \mathbf{w} \in \operatorname{range}(M_{21}) \oplus \operatorname{range}(A_{21}) \right\}.$$

The function $f_{\tilde{\Lambda}}$ is approximated by interpolation using Chebyshev nodes $\{\xi_i\}_{i=1}^N$ on $(0, \Lambda)$:

$$f_{\tilde{\Lambda}}(t) \approx \sum_{i=1}^{N} f_{\tilde{\Lambda}}(\xi_i)\ell_i(t), \quad \ell_i(t) = \prod_{j \neq i} \frac{t - \xi_i}{\xi_j - \xi_i}.$$

Let $\{\mathbf{p}_j\}_{j=1}^r$ be a basis of $\operatorname{range}(\mathsf{M}_{21}) \oplus \operatorname{range}(\mathsf{A}_{21})$. We define a complementing subspace containing the interpolant of $f_{\tilde{\Lambda}}(t)\mathbf{w}$ for any $t \in (0, \Lambda)$ and $\mathbf{w} \in \operatorname{range}(\mathsf{M}_{21}) \oplus \operatorname{range}(\mathsf{A}_{21})$ as

$$\mathcal{W}_2 = \operatorname{span}\left\{ f_{\tilde{\Lambda}}(\xi_i)\mathbf{p}_j \;\middle|\; i = 1 \ldots N,\ j = 1 \ldots r \right\}.$$

The approximation error (4.3) can be analysed using standard interpolation error estimates leading to Theorem 4.4 in Publication IV:

$$\frac{|\lambda - \tilde{\lambda}|}{\lambda} \leq C\gamma^3 \left[4(\gamma - 1)\right]^{-2N-2},$$

where $\gamma := \tilde{\Lambda}/\Lambda$ is called the *oversampling parameter* and $\tilde{\lambda} \in \sigma_{\mathcal{V}}(\mathsf{A}, \mathsf{M}) \cap (0, \Lambda)$ is the eigenvalue approximating $\lambda \in \sigma(\mathsf{A}, \mathsf{M}) \cap (0, \Lambda)$. This gives

an exponential convergence with respect to the number of interpolation points N. The convergence rate depends on the oversampling parameter which should be chosen as $\gamma > 5/4$. In the implementation discussed in Publication IV, the vectors $\mathbf{p}_j$ are the non-zero columns of M_{21} and A_{21}. A basis for the Ritz space $\mathcal{V}_2$ is obtained from the matrix

$$\begin{bmatrix} \mathbf{v}_1 & \dots & \mathbf{v}_{K(\tilde{\Lambda})} & f_{\tilde{\Lambda}}(\xi_1)\mathbf{p}_1 & \dots & f_{\tilde{\Lambda}}(\xi_N)\mathbf{p}_r \end{bmatrix},$$

using SVD. See Publication IV for details.

4.2 Distributed solution of eigenvalues

Let us look at solving (3.3) using multiple workstations or a cloud computing service. In order to efficiently utilise the computational power, the problem needs to be split into several subproblems that can be computed independently on each worker node. A natural way to do this is to partition the domain Ω and let each node compress the amount of information related to its assigned subdomain. But how do we achieve this when each eigenmode has predominantly global behaviour?

The CPI method described in Section 4.1 can be generalised for an arbitrary amount of subdomains. However, the amount of degrees of freedom on the interfaces of a complex 3D mesh is so large that the SVD becomes infeasible to compute.

In order to reduce the amount of computation required, an *extended subdomain* is created for each subdomain, see Figure 4.3. A different representation formula is considered for mapping data from the boundary of the extended subdomain to the interior of the subdomain. Due to the regularity properties of the Laplace operator, the λ-dependent mapping is compact for any parameter value. Using a linearisation step with interpolation, a compact linear operator describing the mapping of boundary data associated with the spectral interval of interest into the subdomain can be constructed for each subdomain. SVD is used to create a low dimensional basis for the range of this operator. Using an appropriate orthogonalisation of the basis, a low-dimensional eigenvalue problem is assembled on the master node, which only has to compute the off-diagonal entries of the reduced-order mass and system matrices.

The reduced eigenvalue problem has sparse diagonal blocks but each off-diagonal block corresponding to overlapping subdomains is full. An example of the sparsity is shown in Figure 4.2.

We will now look at each step described above in more detail to piece together the method. For simplicity, we consider the case $\Gamma_D = \partial\Omega$.

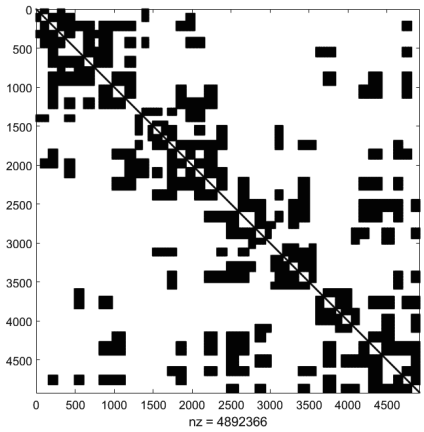

Figure 4.2. An illustration of the non-zero entries of a PU-CPI reduced order stiffness matrix. The full blocks correspond to neighbouring subdomains.

4.3 Subdomains and extensions

Let $\{U^{(p)}\}_{p=1}^{M}$ be an open cover of Ω,

$$\Omega = \bigcup_{p=1}^{M} U^{(p)}.$$

For $p = 1, \ldots, M$, we associate an extended subdomain $\widehat{U}^{(p)}$ with $U^{(p)}$ satisfying

$$\{x \in \Omega \mid dist(x, U^{(p)}) < r\} \subset \widehat{U}^{(p)}.$$

Here $r > 0$ is a user-defined parameter. A non-unique definition is used due to the FEM discretisation, where the extended subdomains are chosen as element sets whose boundaries do not follow the level sets of the distance function.

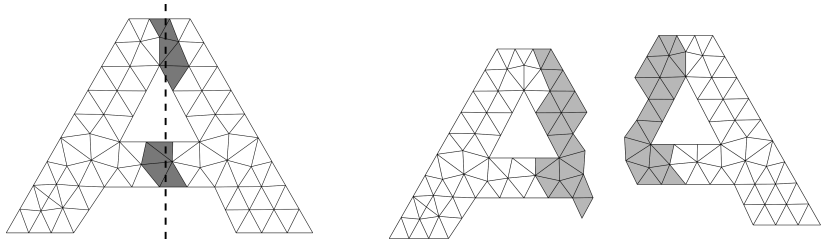

Figure 4.3. A two-dimensional domain split into two subdomains $\Omega_1,\ \Omega_2$ along the dashed line. The overlapping triangles are shown in dark gray on the left. The subdomains Ω_1 and Ω_2 are shown in white on the right, and the subdomain extensions are shown in light gray.

4.4 Continuous representation formula

Next, we derive a representation formula similar to (4.4) in a continuous setting. We focus on a single subdomain U and its extended subdomain $\widehat{U}$. For simplicity, we assume $\partial\widehat{U} \cap \partial\Omega = \emptyset$. Let $(\lambda, u) \in (0, \Lambda) \times H_0^1(\Omega)$ be a solution to (3.3), and split the eigenfunction as follows:

$$u|_{\widehat{U}} = u_0 + Eu_B, \tag{4.7}$$

where $u_0 \in H_0^1(\widehat{U})$ and $u_B = \gamma_{\partial\widehat{U}} u$. Here $\gamma_{\partial\widehat{U}}$ is the trace operator and E its right inverse satisfying $Eu_B|_U = 0$. Hence, we have $u|_U = u_0|_U$. Choosing $v \in H_0^1(\widehat{U})$ and using the splitting in (4.7), problem (3.3) becomes

$$\int_{\widehat{U}} \nabla u_0 \cdot \nabla v - \lambda u_0 v \,\mathrm{d}x = -\int_{\widehat{U}} \nabla Eu_B \cdot \nabla v - \lambda (Eu_B) v \,\mathrm{d}x. \tag{4.8}$$

We call $(\lambda, u_B) \mapsto u_0|_U = u|_U$ implicitly defined by (4.8) the *continuous representation mapping*. This mapping is not well defined if λ is an eigenvalue of the Dirichlet Laplacian in $\widehat{U}$. To define the analytic part of the representation mapping, the function u_0 is partially solved from (4.8) using an eigenbasis $\{v_k\}$ of $H_0^1(\widehat{U})$ with corresponding eigenvalues $\{\mu_k\}$ satisfying

$$\int_{\widehat{U}} \nabla v_k \cdot \nabla v \,\mathrm{d}x = \mu_k \int_{\widehat{U}} v_k v \,\mathrm{d}x \quad \text{for each } v \in H_0^1(\widehat{U}), \quad \|v_k\|_{L^2(\widehat{U})} = 1.$$

Choosing $v = v_k$ in (4.8) gives

$$(\mu_k - \lambda) \int_{\widehat{U}} u_0 v_k \,\mathrm{d}x = -\int_{\widehat{U}} \nabla Eu_B \cdot \nabla v_k - \lambda (Eu_B) v_k \,\mathrm{d}x.$$

Since $u_0 \in H_0^1(\widehat{U})$, we can use the eigenfunction basis representation $u_0 = \sum_{j=1}^{\infty} \alpha_j v_j$. Using the orthogonality of the eigenfunctions allows us to solve the coefficients α_j when $\lambda \notin \sigma(H_0^1(\widehat{U}))$:

$$\alpha_j = \frac{1}{\mu_k - \lambda} \int_{\widehat{U}} -\nabla Eu_B \cdot \nabla v_k + \lambda (Eu_B) v_k \,\mathrm{d}x.$$

Here $\sigma(H_0^1(\widehat{U}))$ denotes the family of eigenvalues of the Dirichlet Laplacian in $\widehat{U}$. Through this identity, we define an operator-valued function $Z : (0, \Lambda) \to \mathcal{B}(H^{1/2}(\partial\widehat{U}), H^1(\widehat{U}))$ as

$$Z(t) w_B := \sum_{k=K(\tilde{\Lambda})+1}^{\infty} \frac{v_k}{\mu_k - t} \int_{\widehat{U}} -\nabla Ew_B \cdot \nabla v_k + t (Ew_B) v_k \,\mathrm{d}x, \tag{4.9}$$

where $\tilde{\Lambda} > \Lambda$ and $K(t) := \#\{\lambda \mid \lambda \in \sigma(H_0^1(\widehat{U})),\ \lambda < t\}$. The solution u_0 in $\widehat{U}$ is then given by

$$u_0 = \sum_{k=1}^{K(\tilde{\Lambda})} \alpha_k v_k + Z(\lambda) u_B. \tag{4.10}$$

The restriction of u to U is given by the *continuous representation formula*:

$$u|_U = \sum_{k=1}^{K(\tilde{\Lambda})} \alpha_k v_k|_U + Z_U(\lambda) u_B, \tag{4.11}$$

where $Z_U(t)w_B := (Z(t)w_B)\,|_U$ is the analytic part of the continuous representation mapping. The reason for defining the solution in U as a restriction from an extended subdomain $\widehat{U}$ is that the operator $Z_U(t)$ is compact for every $t \in (0, \Lambda)$ due to the regularity properties of the Laplace operator. Thus, $Z_U(t)$ has a finite rank approximation for each $t \in (0, \Lambda)$. In the next section, we present a way to approximate the ranges of these operators.

4.5 Partition of Unity CPI

We proceed to define the PU-CPI method subspace $\widetilde{\mathcal{V}}$. Let $\widetilde{\mathcal{V}}^{(p)} \subset H^1(U^{(p)})$ be local Ritz spaces associated with the subdomains $U^{(p)}$. The space $\widetilde{\mathcal{V}}$ is constructed using a variant of the partition of unity method originally introduced by Babuška and Melenk [7]. Recall the open cover $\{U^{(p)}\}_{p=1}^M$ of Ω. For each p, define a stitching operator $R^{(p)} \in \mathcal{B}(H^1(U^{(p)}), H^1(\Omega))$ such that

$$(R^{(p)} w^{(p)})|_{\Omega \setminus U^{(p)}} = 0 \quad \text{and} \quad \sum_{p=1}^{M} R^{(p)}(w|_{U^{(p)}}) = w,$$

for each $w^{(p)} \in H^1(U^{(p)})$ and $w \in H^1(\Omega)$. These operators can be constructed in FEM by simply setting the coefficients of basis functions not fully supported on $U^{(p)}$ to zero.

The PU-CPI method subspace is defined as

$$\widetilde{\mathcal{V}} := \left\{ w \in H_0^1(\Omega) \;\middle|\; w = \sum_{p=1}^{M} R^{(p)} w^{(p)} \quad \text{for} \quad w^{(p)} \in \widetilde{\mathcal{V}}^{(p)} \right\}. \tag{4.12}$$

In Publication V, the relative eigenvalue error is bounded by a multiplicative constant and the sum of local approximation error terms

$$\mathcal{E}(u, U^{(p)}) = \min_{w \in \widetilde{\mathcal{V}}^{(p)}} \int_{U^{(p)}} \left| \nabla R^{(p)} (u|_{U^{(p)}} - w) \right|^2 \, dx. \tag{4.13}$$

The local Ritz spaces $\widetilde{\mathcal{V}}^{(p)}$ are designed to minimise the local approximation error terms related to eigenfunctions u associated with the spectral interval of interest $(0, \Lambda)$. According to (4.11), we use the splitting $\widetilde{\mathcal{V}}^{(p)} = E_{\tilde{\Lambda}}^{(p)} \oplus \mathcal{W}^{(p)}$. Similar to Section 4.1, $\mathcal{W}^{(p)}$ is chosen to approximate the space

$$\left\{ Z_U(t) w_B \;\middle|\; t \in (0, \Lambda),\ w_B \in H^{1/2}(\partial \widehat{U}^{(p)}) \right\}.$$

To construct $\mathcal{W}^{(p)}$, we first perform a *linearisation step*. Define $B \in \mathcal{B}([tr(\mathcal{V}(U))]^N, \mathcal{V}(U)))$ as

$$B\mathbf{w}_B = \sum_{i=1}^{N} Z_U(\xi_i) w_{B,i} \quad \text{where} \quad \mathbf{w}_B = (w_{B,1}, \ldots, w_{B,N}). \tag{4.14}$$

Denote $\mathbf{w}_B^\ell(t) = [\ell_1(t)w_B, \ldots, \ell_N(t)w_B]$. Then $B\mathbf{w}_B^\ell(t) = \sum_{i=1}^N \ell_i(t) Z_U(\xi_i) w_B$. Thus, the Lagrange interpolation polynomials of $Z_U(t)$ for $t \in (0, \Lambda)$ can be represented through B. Since B is a compact linear bounded operator, it can be approximated by a finite rank operator $\widehat{B}$. Thus, we choose $\mathcal{W}^{(p)} = range(\widehat{B})$. The local approximation error terms (4.13) are bounded by a finite rank approximation error and the interpolation error. For more details, see Publication V.

A similar construction is feasible in the context of finite element method, where $H_0^1(\Omega)$ is replaced by a finite element space $\mathcal{V}_h$. The operator $\widehat{B}$ is formed using SVD. An example of an implementation of the method is given in Publication V, where the authors solve three-dimensional eigenproblems on a cluster of 26 networked workstations. In the most demanding examples, the number of degrees of freedom was significantly higher than a single workstation could manage.

Bibliography

[1] D. Aalto, O. Aaltonen, R-P Happonen, P. Jääsaari, A. Kivelä, J. Kuortti, J-M Luukinen, J. Malinen, T. Murtola, R. Parkkola, J. Saunavaara, T. Soukka, and M. Vainio. Large scale data acquisition of simultaneous MRI and speech. *Applied Acoustics*, 83:64–75, 2014.

[2] D. Aalto, J. Helle, A. Huhtala, A. Kivelä, J. Malinen, J. Saunavaara, and T. Ronkka. Algorithmic surface extraction from MRI data: modelling the human vocal tract. In *Proceedings of BIODEVICES 2013*, 2013.

[3] A. Hannukainen, T. Lukkari, J. Malinen, and P. Palo. Vowel formants from the wave equation. *The Journal of the Acoustical Society of America*, 122(1):EL1–EL7, 2007.

[4] J. Harrington and S. Cassidy. *Techniques in Speech Acoustics*. Text, Speech and Language Technology. Springer, 1999.

[5] A. V. Knyazev and J. E. Osborn. New a priori FEM error estimates for eigenvalues. *SIAM Journal on Numerical Analysis*, 43(6):2647–2667, 2006.

[6] P. Ladefoged and S.F. Disner. *Vowels and Consonants*. Wiley, 2012.

[7] J.M. Melenk and I. Babuška. The partition of unity finite element method: Basic theory and applications. *Computer Methods in Applied Mechanics and Engineering*, 139(1):289 – 314, 1996.

[8] B. N. Parlett. *The Symmetric Eigenvalue Problem*. Prentice-Hall, Inc., 1998.

[9] I. L. Pykett. NMR Imaging in Medicine. *Scientific American*, 246(5):78–91, 1982.

[10] M. Stone and T. H. Shawker. An ultrasound examination of tongue movement during swallowing. *Dysphagia*, 1(2):78, 06 1986.

[11] S. Vallaghé, P. Huynh, D. J. Knezevic, L. Nguyen, and A. T. Patera. Component-based reduced basis for parametrized symmetric eigenproblems. *Advanced Modeling and Simulation in Engineering Sciences*, 2(7), 2015.

Aalto-DD 151/2020

ISBN 978-952-64-0066-2 (printed)
ISBN 978-952-64-0067-9 (pdf)
ISSN 1799-4934 (printed)
ISSN 1799-4942 (pdf)

Aalto University
School of Science
Department of Mathematics and Systems Analysis
www.aalto.fi

BUSINESS + ECONOMY

ART + DESIGN + ARCHITECTURE

SCIENCE + TECHNOLOGY

CROSSOVER

DOCTORAL DISSERTATIONS